Supplementary Material

Supplementary Figure 1. *NOS2*$^{-/-}$ mice develop an analogous Ghon complex after infection in the ear dermis and show dissemination of Mtb to the lung. **(A)** WT and *NOS2*$^{-/-}$ mice were infected in the ear dermis with 10^4 Mtb and colony-forming units (c.f.u.) from homogenates of ear dermis, dermis draining auricular lymph node (dLN) and spleen were enumerated on days 1, 7, 14, 28 and 50 p.i. C.f.u. are shown at each time point as mean ± SEM (n=5). After day 14 p.i., *NOS2*$^{-/-}$ mice showed diminished ability to control Mtb replication at both sites compared to WT. **(B)** Hematoxylin and eosin (HE) staining of dLN at days 28 and 56 p.i. demonstrated necrosis in *NOS2*$^{-/-}$, but not WT mice (magnification x 25). (**C**) Higher magnification revealed non-ordered granulomatous necrosis with a predominantly neutrophilic infiltrate (x 200).

Supplementary Figure 2. Dermal-infected *NOS2*$^{-/-}$ but not WT mice demonstrate steady-stae Mtb infection of the lung. Lung c.f.u. from WT and *NOS2*$^{-/-}$ mice at days 1, 7, 14, 28 and 56 p.i. after dermal Mtb infection are shown as mean ± SE (n=5). WT mice showed an absence of cultivatible c.f.u. in the lung after day 14 p.i. while *NOS2*$^{-/-}$ mice showed stable c.f.u. in the lung after day 14 p.i. indicating establishment of a stable Mtb infection.

Supplementary Figures 3 and 4. Dermal-infected (black bars) WT and *NOS2*$^{-/-}$ mice develop robust Mtb-specific T-cell responses in the lung in the face of reduced bacterial load compared to aerosol-infected mice (white bars). Cells purified from the lungs of infected mice at days 14 and 28 p.i. were stimulated for 6 h with ESAT-6 peptide, PPD or medium only and stained for intracellular expression of IFN-γ and TNF-α and analyzed by FACS. Percentage $CD4^+$-gated T cells staining for IFN-γ or IFN-γ and TNF-α are shown as mean (n=3) ± SEM.

Supplementary Figure 5. Effects of cytokine blocking on development of lung Mtb-specific T-cell responses in dermal-infected *NOS2*$^{-/-}$ mice. Cells purified from the lungs of dermal-infected TNF-α (red bars), IFN-γ-depleted (white bars) or control (non-blocked *NOS2*$^{-/-}$: black bars) mice at day 28 p.i. were stimulated for 6 h with ESAT-6 peptide, PPD or medium only and stained for intracellular expression of IFN-γ and TNF-α and analyzed by FACS. Percentage of $CD4^{+}$-gated T cells staining for IFN-γ or both IFN-γ and TNF-α shown as mean (n=3) ± SEM.

Supplementary Figure 6. Caseous granulomas in *NOS2*$^{-/-}$ mice (d56 p.i.) resemble caseating granulomas observed during human tuberculosis. **(A)** Staining with anti-CD3 and anti-F4/80 mAbs revealed T cells and macrophages encircling the central necrotic core in granulomas of *NOS2*$^{-/-}$ mice. Similar configurations of T cells and macrophages within human caseous granulomas during active tuberculosis were observed. **(B)** Competitive microarray analyses of cDNA transcribed from pooled mRNA purified from lungs of mice (n=3) day 28 p.i. Numbers are representative of fold change in ctsg, NE and Prtn3 expression of *NOS2*$^{-/-}$ vs WT or IFN-γ-depleted *NOS2*$^{-/-}$ vs control *NOS2*$^{-/-}$ mice. Fold changes >2 and $p<0.01$ are highlighted in blue.

Supplementary Figure 7. Comparison of myeloperoxidase (MPO) staining in the lungs of *NOS2*$^{-/-}$ mice after aerosol Mtb infection (d30 p.i.) or dermal infection with IFN-γ or TNF-α blocking (d56 p.i.) (n=5). Aerosol-infected mice demonstrated strong MPO staining due to marked neutrophillic infiltrates into the lung. In contrast, caseous granulomas in the lung after dermal infection with IFN-γ or TNF-α blocking contained fewer neutrophils with MPO staining markedly weaker. Top panels x 100 and lower panels x 400 magnification.

Supplementary Figure 8. Exogenous h-ctsg reduces intracellular growth of Mtb in vitro and AEBSF treatment does not affect bacterial burden in control dermal-infected *NOS2*$^{-/-}$ mice. **(A)** Direct enumeration of c.f.u. from IFN-γ-activated macrophages infected with Mtb (MOI 2, 72 h p.i.) with and without exogenous addition of 10μg/ml h-ctsg (n=5). Data corroborates the reduction in intracellular bacterial growth on addition of h-ctsg observed by measurement of incorporation of [3H] Uracil into bacterial DNA. **(B)** Bacterial burden of tissue homogenates from dermal-infected *NOS2*$^{-/-}$ mice in auricular lymph node (dLN), spleen and lung after twice weekly treatment with AEBSF. C.f.u. at day 56 p.i. are shown as mean ± SEM (n=5). **(C)** Measurement of maximum velocity of h-ctsg activity (Vmax) by proteolysis of the chromogenic peptide N-succinyl-Ala-Ala-Pro-Phe-P-Nitroanilide. Vmax of pure h-ctsg correlated linearly with enzyme concentration in the assay.

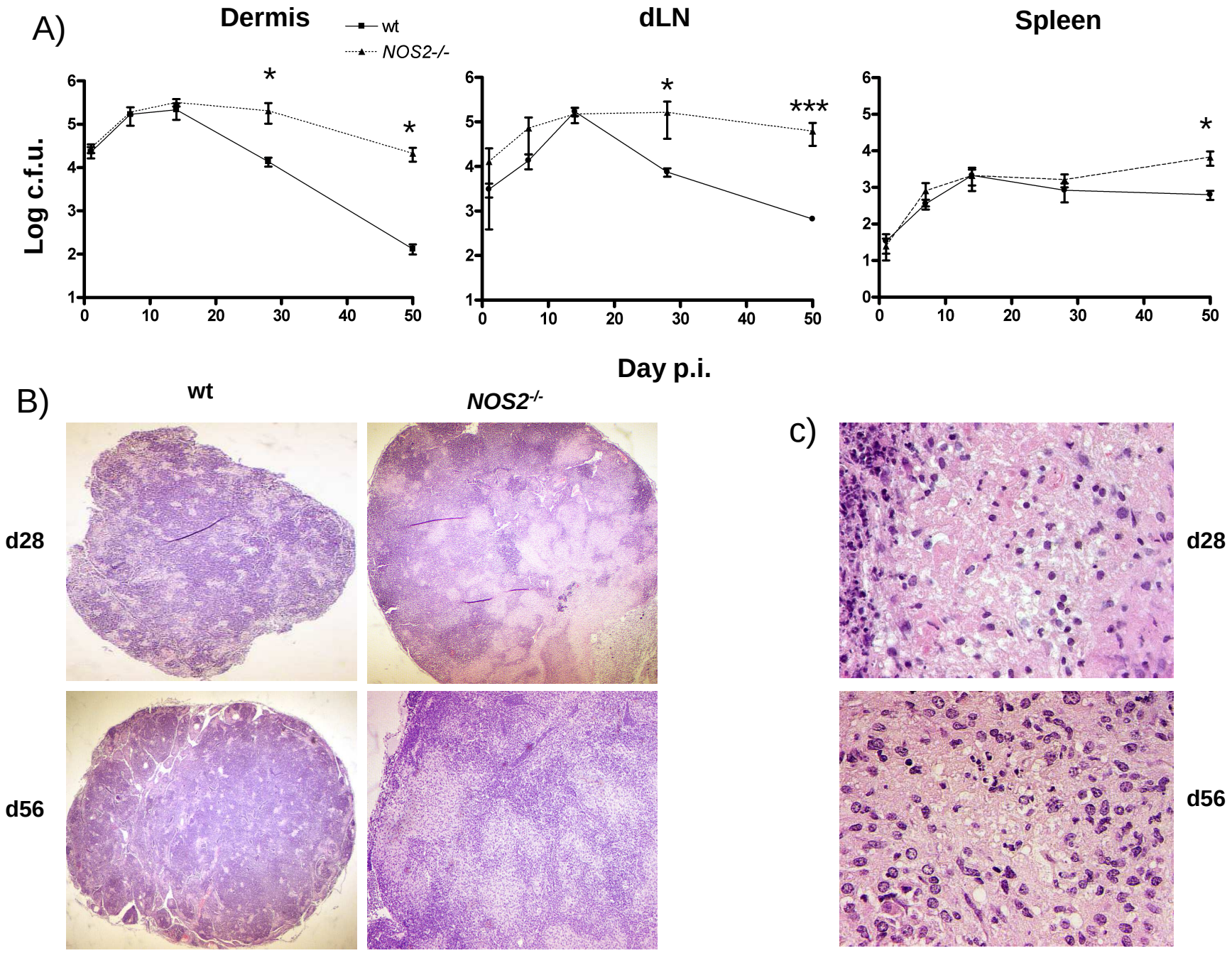

Supplementary Figure. 1

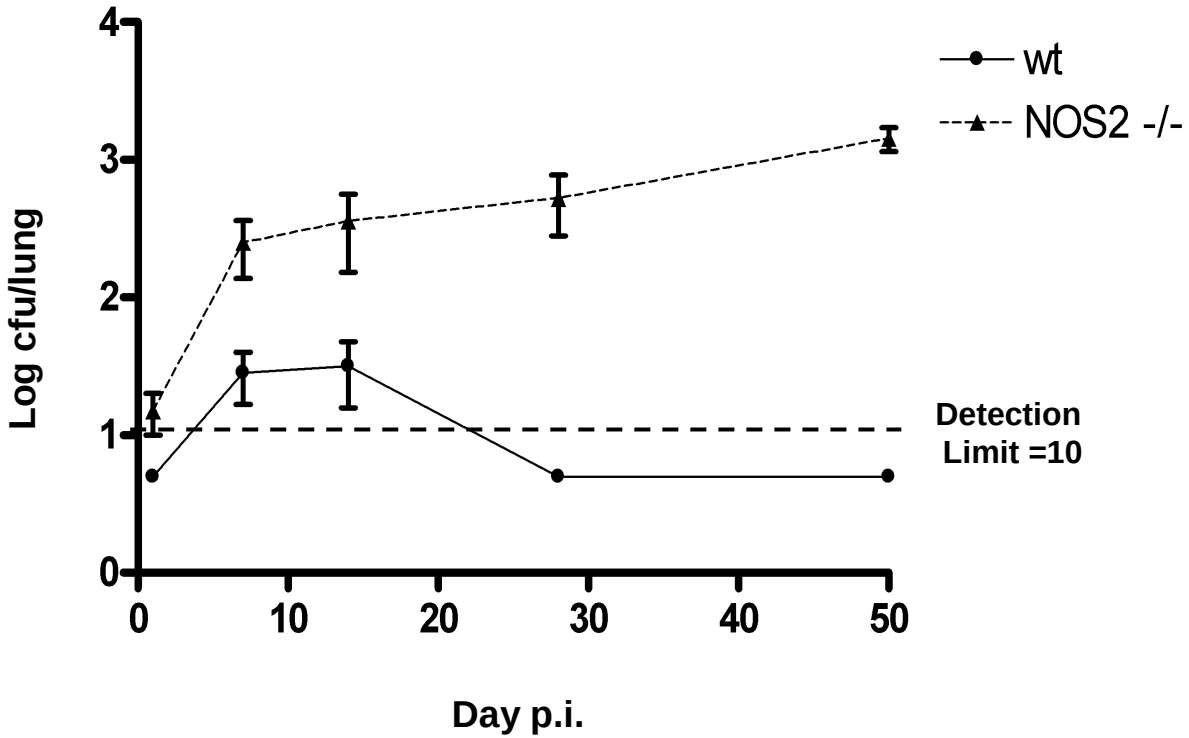

Supplementary Figure. 2

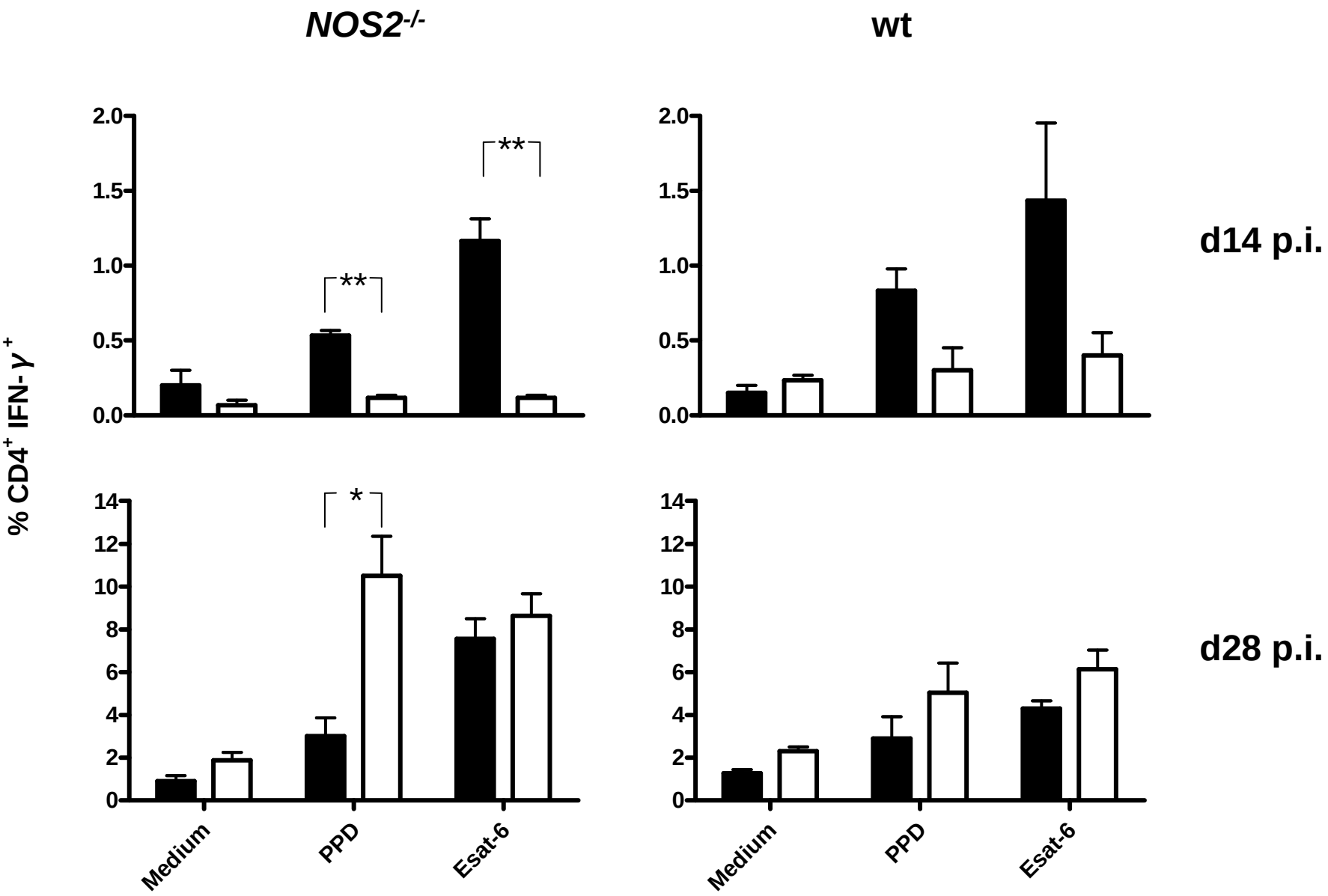

Supplementary Figure. 3

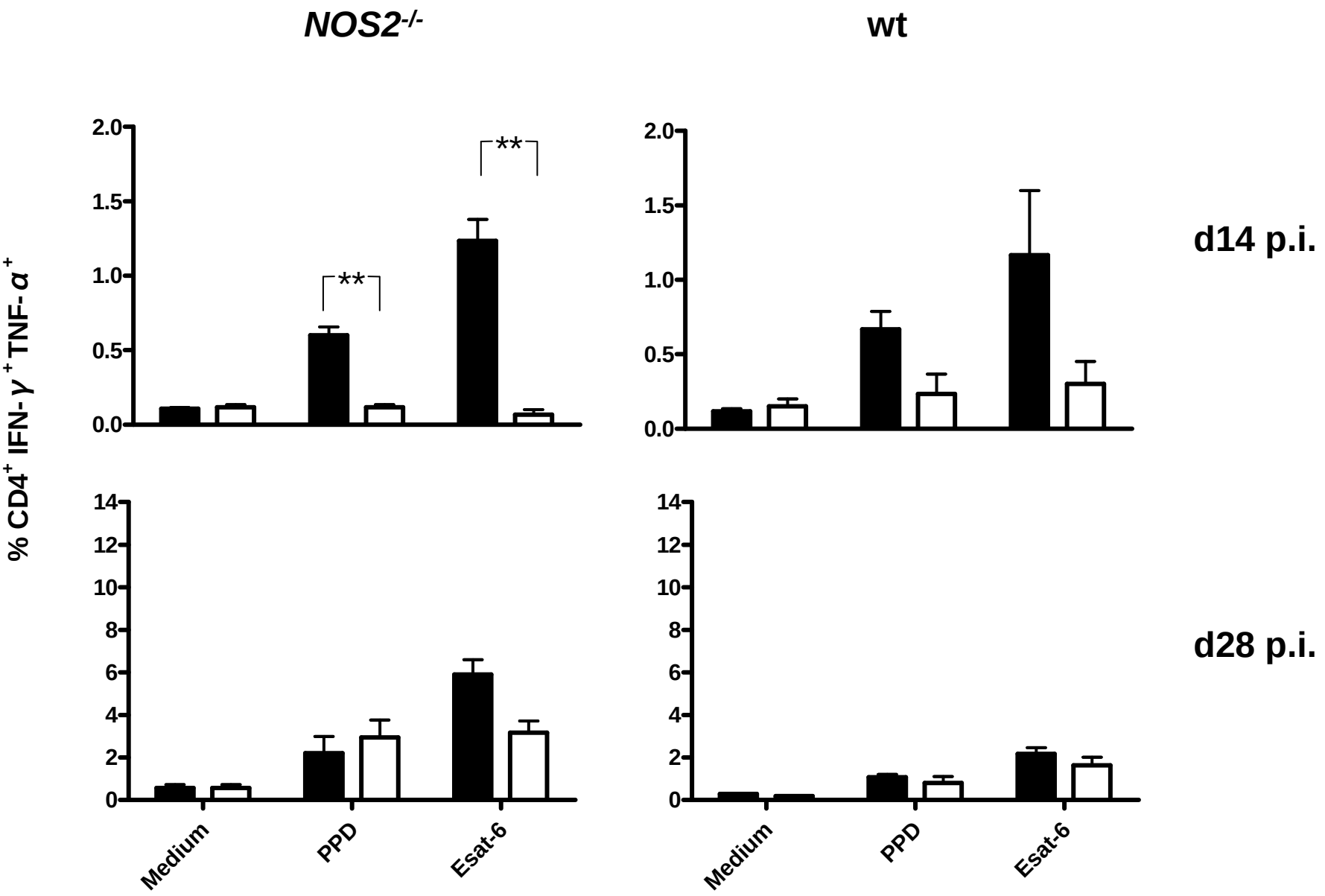

Supplementary Figure. 4

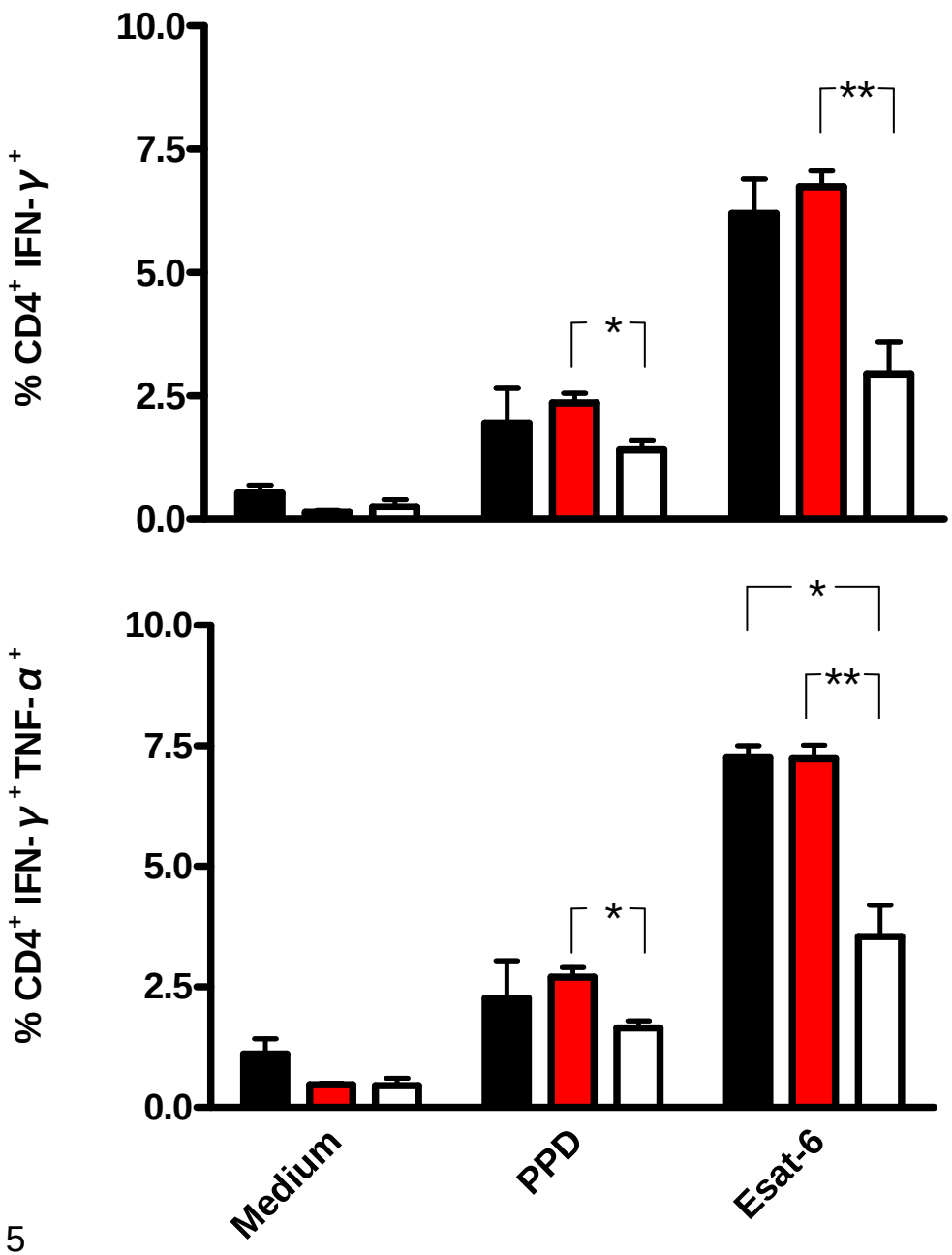

Supplementary Figure. 5

A)

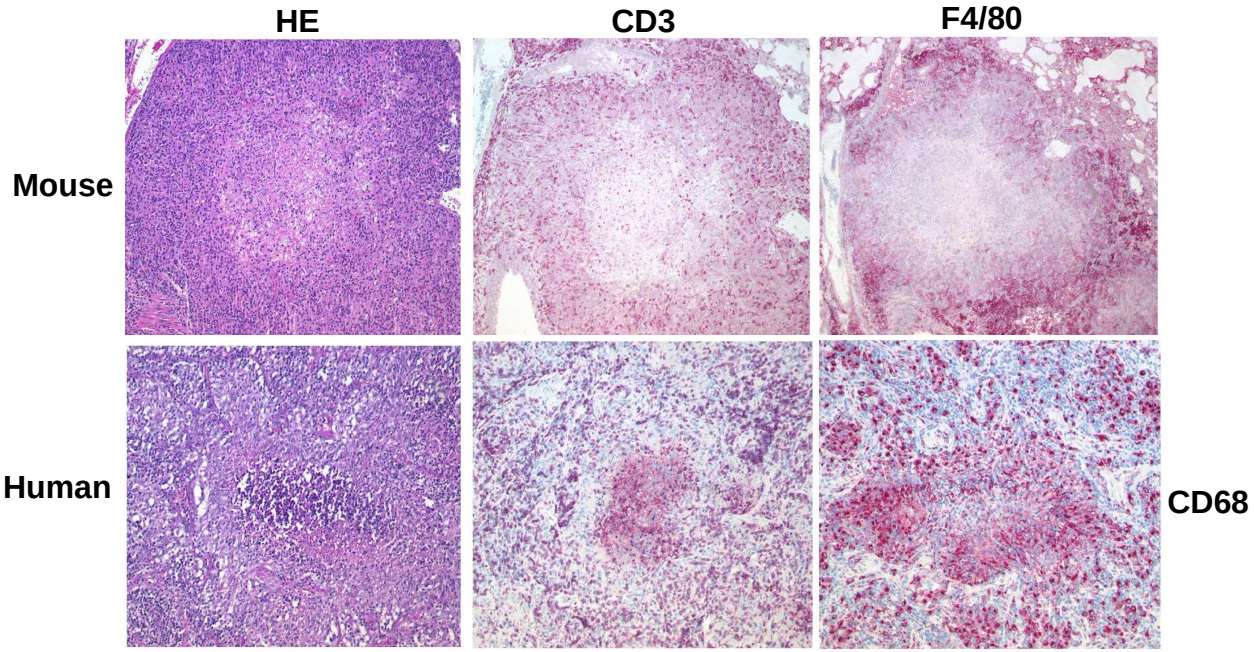

B)

Protease	Class	*NOS2*$^{-/-}$ vs wt	INF-γ -blocked *NOS2*$^{-/-}$ vs *NOS2*$^{-/-}$
Cathepsin G (ctsg)	**Serine**	**5.36**	**12.6**
Neurophil Elastase (ela2)	**“**	**3.85**	**5.87**
Proteinase 3 (Prtn3)	**“**	**2.3**	**6.4**
Cathepsin E (ctse)	**Aspartic**	1.80	1.88
Cathepsin K (ctsk)	**Cysteine**	1,35	-1,96
Calpain 3 (capn3)	**“**	-1,01	1.96

>2 fold, p<0.01

Supplementary Figure. 6

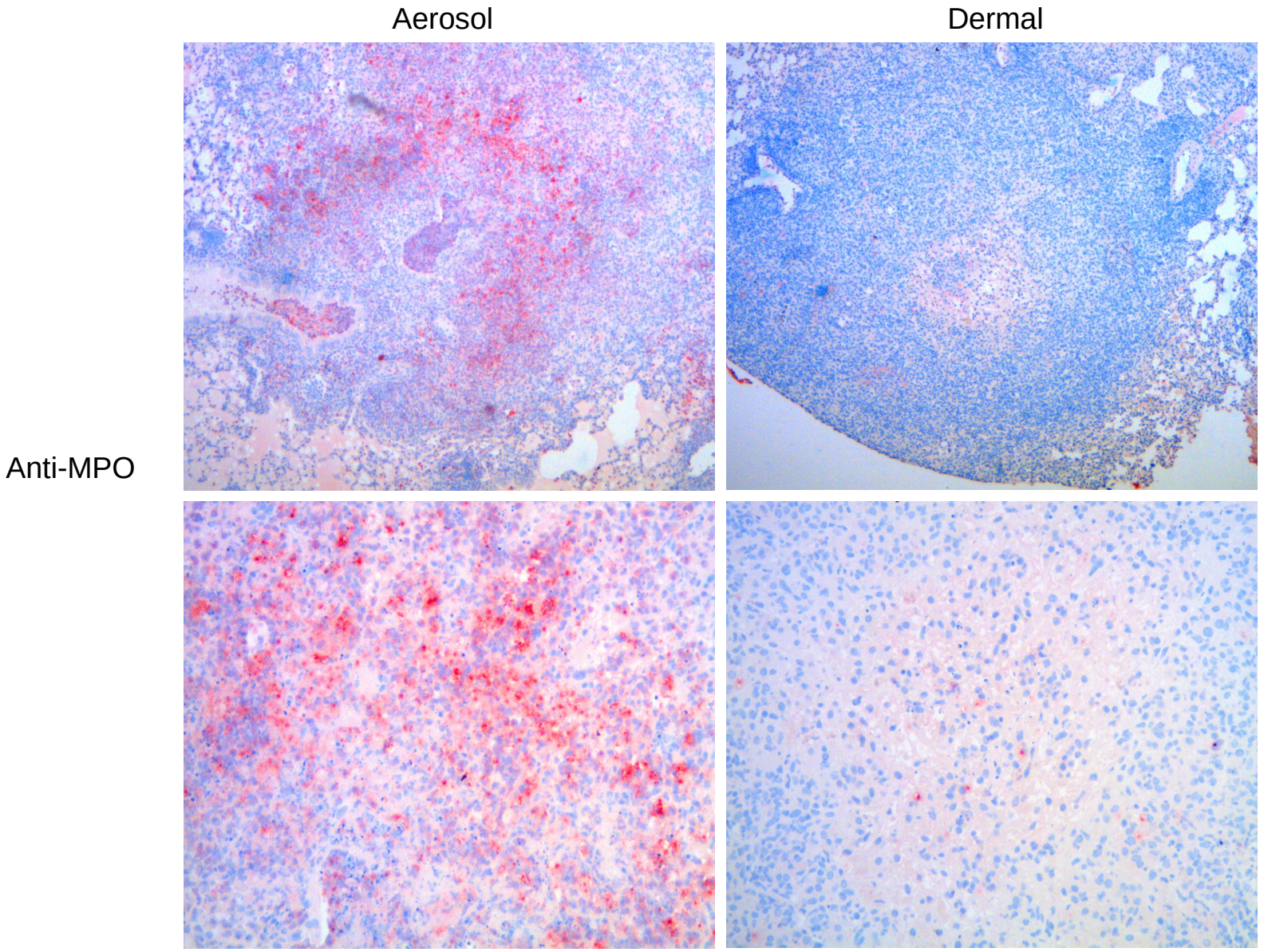

Supplementary Figure. 7

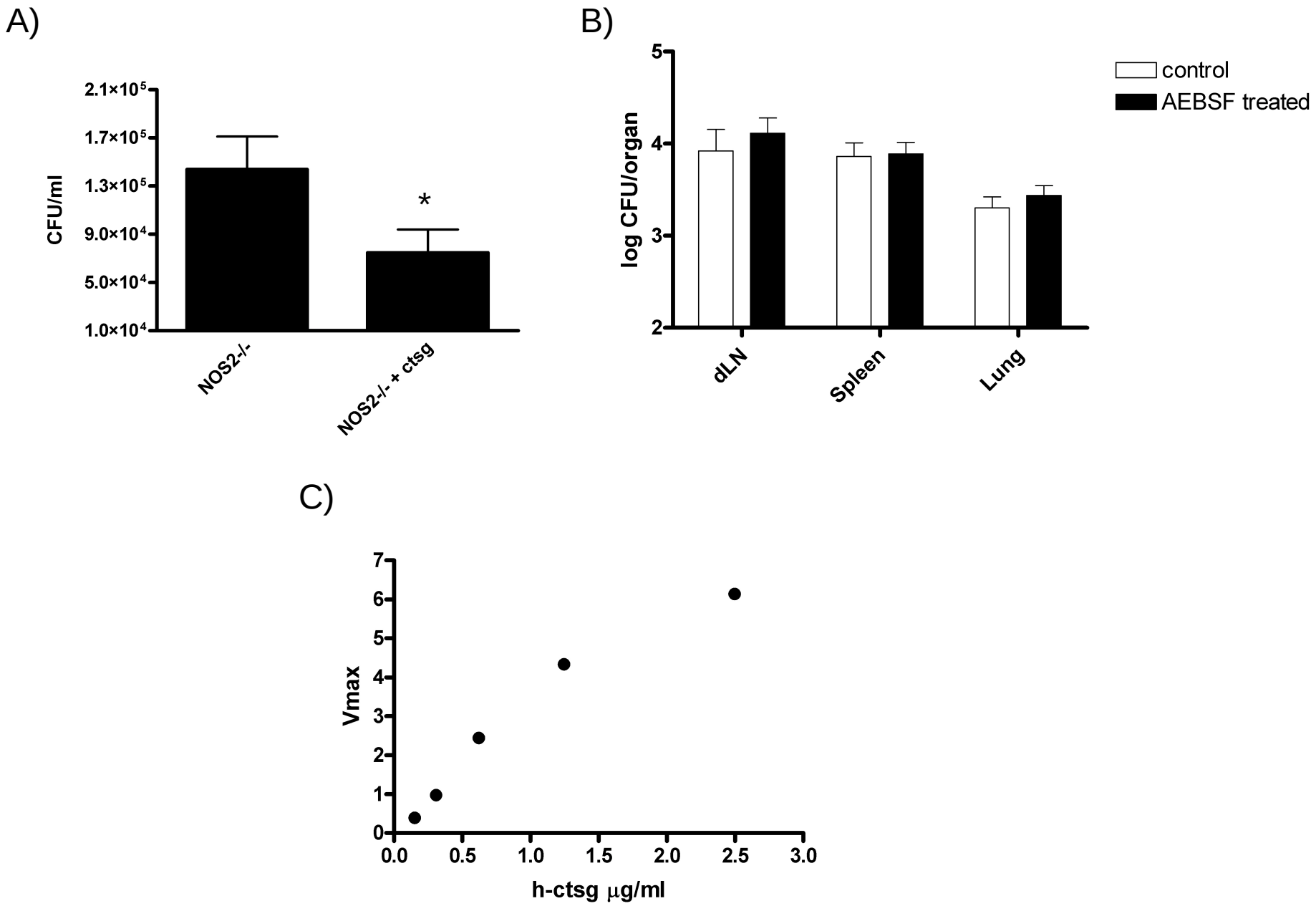

Supplementary Figure. 8